A method for counting mitoses by image processing in Feulgen stained breast cancer sections

ten Kate, T.K.; Belien, J.; Smeulders, A.W.M.; Baak, J.P.A.

Published in:
Cytometry

DOI:
10.1002/cyto.990130305

UB Groningen
UvA Keur
Broerstraat 4
9700 AN Groningen

A078429692 ISN: 682689 RAPDOC (R) **AFGEMELD** NCC/IBL

Aantal afgedrukte pagina's: [ ] (alleen invullen waneer niet gescand maar anders afgedrukt)

Verzoeke te behandelen voor: 08-05-2005 **Ingediend door:** 0004/9999
Datum en tijd van indienen: 24-04-2005 14:11 **Datum plaatsen:** 24-04-2005 14:11 **Type aanvrager:** UKB **I.D.:** UVA KEUR (UB GRONINGEN)

PPN: 840553552

Cytometry : the journal of the International Society for Analytical Cytology Society for Analytical Cytology 1980 New York, NY Liss

Gewenst: 1993-00-00 **Deel:** 14 **Nummer:** 3 **Electronisch leveren (LH=N)**

Auteur:	**Titel van artikel:**	**Pagina's:**
Kate, T.K.ten (ed.)	Method for Counting Mitoses by Image Processing in Feulgen Stained Brea	241-250

Opmerking:
arno ID: 136230

PLANT-HG	MAG	NN37511	Vol. 3 no. 4(1983)-18(1994)
NIOONI			Vol. 19(1995)-31(1998)
WWW			Vol. 27(1997)-

1. ○ origineel gestuurd
2. ○ fotokopie gestuurd
3. ○ overige
4. ○ nog niet aanwezig
5. ○ niet aanwezig
6. ○ niet beschikbaar
7. ○ uitgeleend
8. ○ wordt niet uitgeleend
9. ○ bibliografisch onjuist
10. ○ bij de binder

Fakturen zenden aan: Rijksuniversiteit Groningen
Bibliotheek, Uitleenbureau
Postbus 559
9700AN Groningen

Cytometry 14:241–250 (1993)

Method for Counting Mitoses by Image Processing in Feulgen Stained Breast Cancer Sections[1]

T.K. ten Kate, J.A.M. Beliën, A.W.M.Smeulders, and J.P.A. Baak[2]

Department of Pathology, Free University (T.K.t.K., J.A.M.B., J.P.A.B.) and Faculty of Mathematics and Computer Science and Faculty of Biology, University of Amsterdam (A.W.M.S.), Amsterdam, The Netherlands

Received December 18, 1991; accepted October 19, 1992

This study describes an image processing method for the assessment of the mitotic count in Feulgen-stained breast cancer sections. The segmentation procedure was optimized to eliminate 95–98% of the nonmitoses, whereas 11% of the mitoses did not survive the segmentation procedure. Contour features and optical density measurements of the remaining objects were computed to allow for classification. Twelve specimens were analyzed, nine used to serve as a training set, and three put aside for later use as independent test set. The fully automatic image processing method correctly classified 81% of the mitoses at the specimen level while inserting 30% false positives. The automatic procedure strongly correlated with the interactive counting procedure (r = 0.98). Although the fully automatic method provided satisfactory results, it is not yet suited for clinical practice. The automated method with an interactive evaluation step gave an accurate reflection of the mitotic count showing an almost perfect correlation with the results of the interactive morphometry (r = 0.998). Therefore this semiautomated method may be useful as prescreening device. © 1993 Wiley-Liss, Inc.

Key terms: Image analysis, tissue section, mitotic count, automatic evaluation, breast cancer

The number of mitoses seen in tissue sections is an important factor in grading many malignancies, especially for the prognosis of breast, ovarian, and other tumors (1,20,22,29). Also, mitotic activity is a method to evaluate the rate of proliferation of tumors. Usually, the proliferative activity of tissue is expressed as the mitotic activity index, defined as the number of mitoses detected in a confined and well-defined microscopic area divided by a measure for that area. Classifications may fall into low, moderate, or high mitotic rate (29). To assess the proliferative activity of tumor cells, the mitotic count is related to the total number of analyzed nuclei.

Currently, the mitotic activity index is determined by interactively counting the number of mitoses with a grid inserted in the microscope. Standardized slide preparation, careful and reproducible selection of the most cell-rich area of the tumor, a strict protocol for defining mitoses, and controlled microscope conditions are prerequisites for a reliable count. Then it is comparable with findings in other studies and laboratories (2). Despite these precautions, interactive counting of mitosis is still a subjective task and therefore not perfectly reproducible. Furthermore, the work is time-consuming and tedious. At present, determination of the mitotic activity index accounts for a considerable part of the workload in our laboratory. Therefore, automating part of the mitotic counting is a desired goal. In this work, we describe a semiinteractive approach to assess the number of mitoses in tissue sections by image processing on a low cost pathology workstation.

Image analysis of histological sections thus far has mainly focused on the assessment of DNA content (4,13), morphometry of carcinoma cells (28), and methods to measure and express architectural features (7,24–26,31). Image analysis of tissue sections poses complex problems because the cells do not lie loose but may severely overlap, with no clear background, and the appearance of cells is altered through the introduction of cutting artifacts and variation in tissue thick-

[1]This work was supported by grant #28-736 of the Praeventiefonds and sponsored in part by SPIN programs 3DCV and 3DAI.

[2]Address reprint requests to J.P.A. Baak, Department of Pathology, Free University Hospital, de Boelelaan 1117, 1007 MB Amsterdam, The Netherlands.

ness and staining. In the analysis of tissue sections, much attention is paid to the segmentation process as errors in this step heavily influence subsequent feature extraction and eventually the classification process.

To our knowledge, the only study on the automated recognition of mitoses in tissue sections is by Kaman et al. (16). They describe a feasibility study that aimed at keeping the false-negative fraction (missed mitoses) as low as possible. After a global and local segmentation technique, potential mitoses were selected and subsequently classified using contour features. The result was a relatively large net loss of 37% mitoses, whereas 5% of the nonmitotic nuclei survived. Part of these unsatisfactory findings may be explained by a number of factors that complicated that study. First, the staining used was haematoxylin-eosin, which is standard practice in routine pathology but unsuitable for image processing as it severely hampers the segmentation process. Second, the analysis involved a photographic step prior to digitization, which may seriously have degraded the image quality with loss of detail information and nonlinear response in intensity. Third, images were scanned at five bit resolution, severely limiting the measurable contrast and accuracy of optical density values.

In this work, we analyze breast cancer specimens stained with the Feulgen reaction to facilitate the segmentation and to allow for proper optical density measurements. The images are recorded from specimen through a camera-equipped microscope.

MATERIALS AND METHODS

Patient Material

Twelve tissue sections of invasive ductal breast cancer were used in this study. Tissue specimens were fixed in 4% neutral (buffered) formalin at pH = 7.0. It has been hypothesized that mitotic figures disappear due to fixation delay (3). However, recently it has been demonstrated that mitotic figures do not really disappear but mainly become pycnotic and that S-phase fractions do not change as a result of delayed fixation (10). Yet mitotic figures may become more difficult to identify with increased fixation delay. Therefore, all tumors were fixed within 6 h after excision and kept at 4°C in the meantime.

From the paraffin-embedded tissue blocks, 4-μm sections were cut. One slide was haematoxylin-eosin (HE) stained to serve as visual control, and one section of each breast specimen was stained by the Feulgen procedure (11). Based on the outcome of previous interactive mitoses counting, nine specimens were selected having low, moderate, or high mitotic rates (three of each). The nine corresponding Feulgen sections served as a learning set to cover the spectrum of mitosis appearing in breast tumors. The remaining three specimens were put aside to serve as a test set. Under guidance of one of us (J.P.A.B.), areas on the slides of the complete data set were selected to include the most relevant part of the tumor for mitoses counting.

Interactive Procedures

To evaluate the image processing method, interactive mitoses counting was performed on the standard HE and on the Feulgen-stained sections. The HE-prepared slides were used to assess the mitotic activity index (MAI) according to strictly defined criteria (1,2). Careful selection of the measurement area and counting of the mitoses in 10 adjacent microscopic fields were performed by a trained technician, using a 40× objective (NA = 0.75) with a field diameter of 450 μm, yielding the MAI. Specimens with a MAI < 10 were classified as "low MAI," "moderate" when having a MAI between 10 and 20, and "high" with a MAI ≥ 20. The same microscopic fields were selected in the Feulgen-stained adjacent slides for interactive counting as well as image processing. The Feulgen specimens were evaluated by two observers. The correlation between the mitotic counts of the first and the second observer of the entire set was almost perfect ($r = 0.994$). This demonstrates that the interactive counting may serve as a good reference for the image processing methods.

Instrumentation

A microscope TV system was used consisting of an UEM frame (Zeiss, Oberkochen, Germany) equipped with a 40× dry-lens plan objective (N.A. = 0.65), and a TYK91D camera with a chalnicon tube, (Bosch, Stuttgart, Germany). The slide was moved with an automatic scanning stage (Märzhäuser, Wetzlar, Germany) with a step size of 0.25 μm; and focusing used an autofocus device (Zeiss) operating on the TV signal. The specimens were illuminated with a halogen light source, using a monochrome filter at the wavelength of the maximum absorption of the Feulgen stain ($\lambda = 550$ nm, $\Delta\lambda = 10$ nm). The images of 512 × 512 elements were digitized with a MATROX video board PIP1024B (Matrox Electronic Systems, Dorval, Quebec, Canada) in an 8-bit grey value resolution. The pixel-to-pixel distance at the specimen level was 0.31 μm. Image processing was performed on a SUN386i (Sun Microsystems, Mountain View, CA) running under the UNIX operating system with a color monitor at a spatial resolution of 1,152 × 900 in 8 bit.

The automatic mitoses recognizer was developed and evaluated using the multilevel interactive image processing environment SCILAIM (17). This software package offers a large set of basic image processing operations and in addition is programmable through a C interpreter. The image processing package is especially effective in the analysis of objects. Image data as well as numerical data resulting from measurements image data can be stored in combined databases.

From the interactive system for pattern recognition, ISPAHAN (14), the Fisher linear discriminant option was used for statistical feature evaluation and classi-

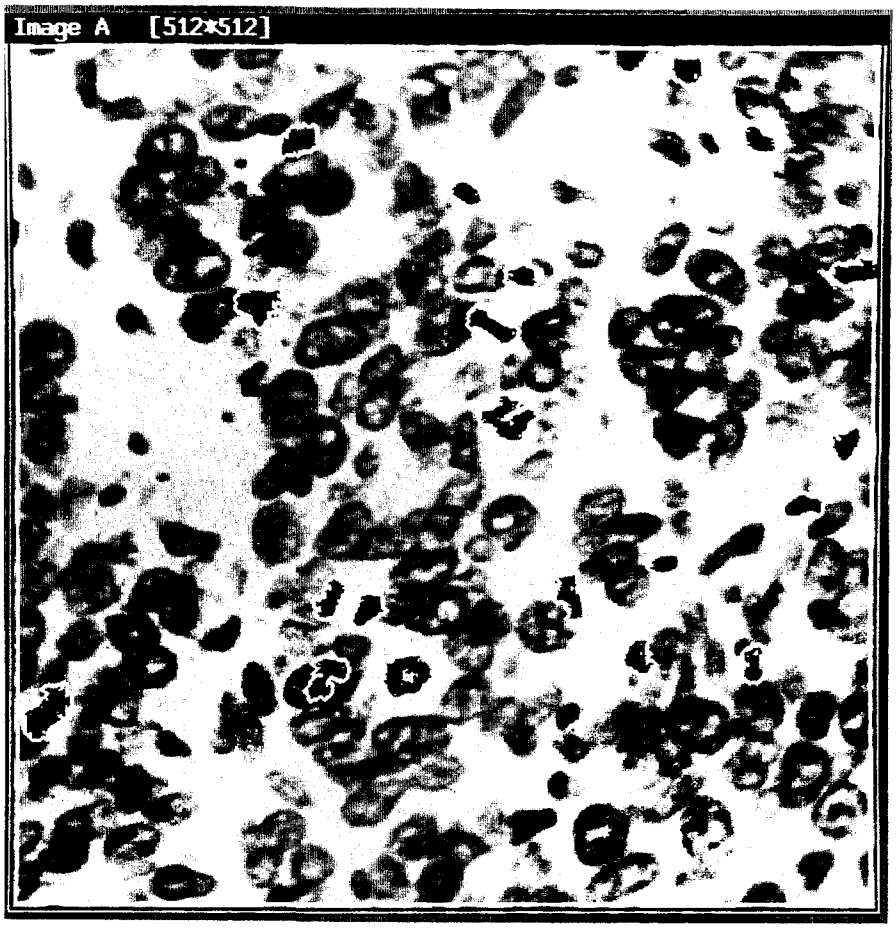

FIG. 1. Result of the region-grow algorithm, showing overlaying contours of microscopic image containing mitoses (objective 40×, NA 0.65).

fication. Linear regression analysis was carried out with the BMDP statistical software package.

Image Processing

Image processing favoured the detection of mitotic figures to achieve successful discrimination between mitoses and other objects such as artefacts and nuclei of inflammatory cells. Mitoses appear as compact and highly dense objects, usually showing hairy extensions at the boundary. They appear in various shapes and sizes, depending on the internal state of the cell, the phase of the division when the mitosis was captured, the cutting angle, and preparational factors. They may appear as almost perfectly circular, rod shape, or, rarely, propeller shape. Sometimes the mitosis appears loose in the field of view where the surrounding cells are more or less tightly packed. However, mitoses may overlap with other nuclei, ranging from barely touching to completely overlapping. The segmentation of these complex images in tissue section poses problems that are difficult to solve. In addition, artefacts, nuclei of inflammatory cells, and dense cell fragments may closely resemble a mitosis.

Simple thresholding of the image was not sufficient for properly detecting mitoses, so region growing was selected as an alternative segmentation approach, which adapts itself locally. Using the fact that mitoses are particularly compact and dense objects, the darkest pixel is used as the starting point for the region growing algorithm. Starting from such a "seed" point, the initial region grows by aggregating pixels that have similar properties. Connected pixels are assigned to a region only if all following conditions are fulfilled: (1) the candidate pixel is 8-connected to the currently found region, (2) the absolute difference in grey level of the candidate point and the average grey level of the current region do not exceed a predetermined level $P_{average}$, or the gradient at the candidate point is ascending with more than a fixed value $G_{gradient}$, (3) the intensity value of the candidate point must be smaller than the estimated background value $B_{background}$. The parameter $P_{average}$ is set to 10% of the difference between maximum and minimum grey levels in the entire image as a measure of contrast. The value for the parameter $G_{gradient}$ must be substantially higher than the noise level present in the system. Setting $G_{gradient}$

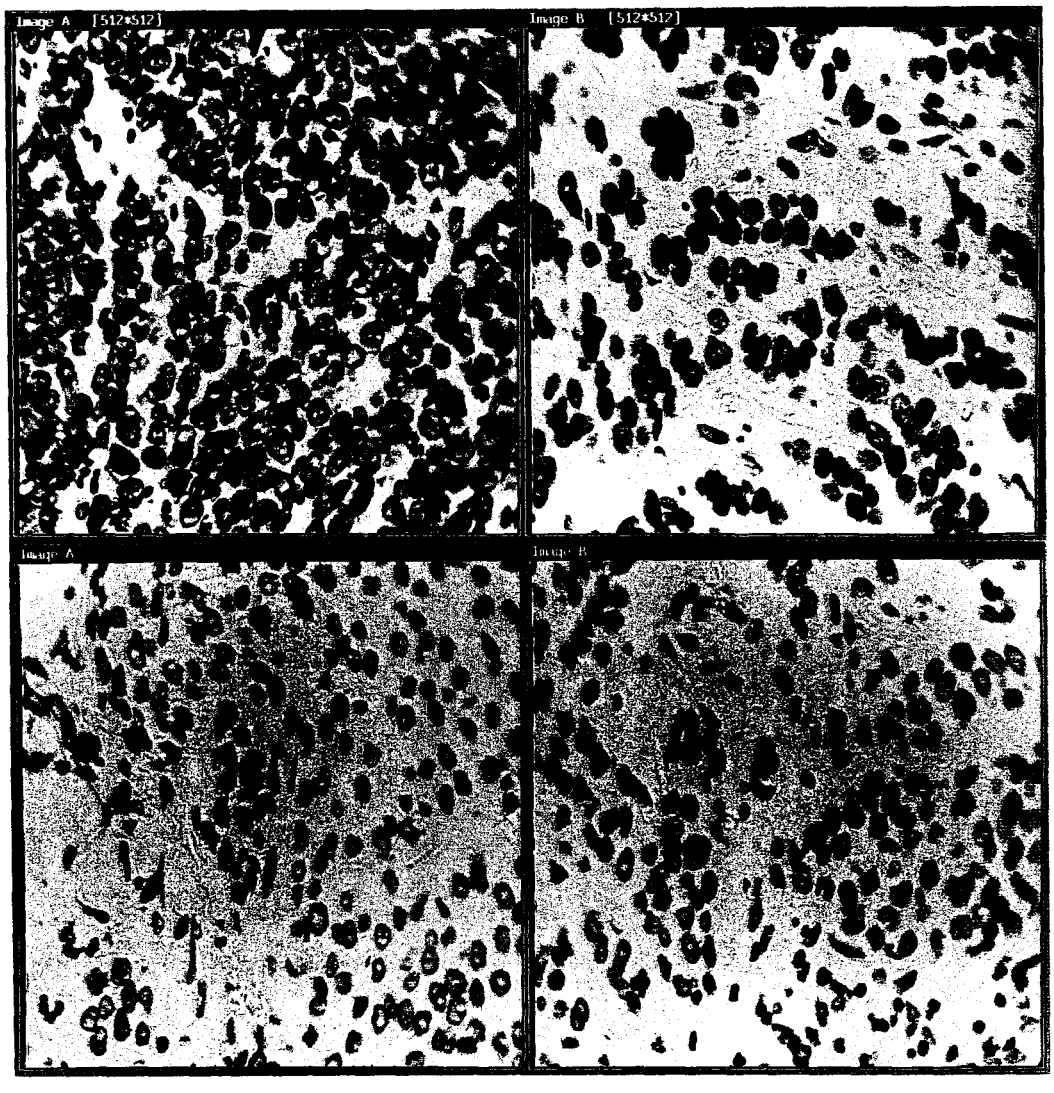

FIG. 2. Images of various specimens showing variety in staining intensity and tumor cell packing (objective 40×, NA 0.65).

at 5% of the dynamic range gave satisfactory results. To prevent the object from growing into the background, $B_{background}$ was determined through an iterative clustering procedure using the grey level histogram (23).

As a result, the region growing algorithm effectively approximated the contours of the mitoses, which is of great importance for the precise computation of the contour features (Fig. 1). This algorithm was integrated in the image processing method to detect the mitoses, consisting of the steps outlined below.

1. Shading correction. Prior to every session, the microscope was carefully adjusted to ensure as standardized conditions as possible. The images were linearly corrected for shading with two empty images according to a procedure detailed previously (18). The corrected grey values thus provide a measure for the local density.

2. (a) Seed points. The seed points for the region growing process were found by applying a rigorous low threshold on the image. The initial threshold is set at 30 for $T < 160$, 50 for $T > 170$, and at 40 for $160 < T < 170$ where T is the level of the isodata algorithm (23). In this way, parts that are sufficiently dense are considered as candidate points and the bulk of nuclei are excluded from further analysis as they no longer participate in the segmentation process. However, setting too low a threshold results in a loss of potential mitoses. Also, the segmentation must be proof against preparational and staining variability of the specimen, see Figure 2. This procedure yielded satisfactory results on the training set in that seeds of all mitoses were retained; this was checked by comparing how many mitoses were detected automatically per image field and interactively in the same field. (b) Region growing. The aggregation process starts from the seed points, and

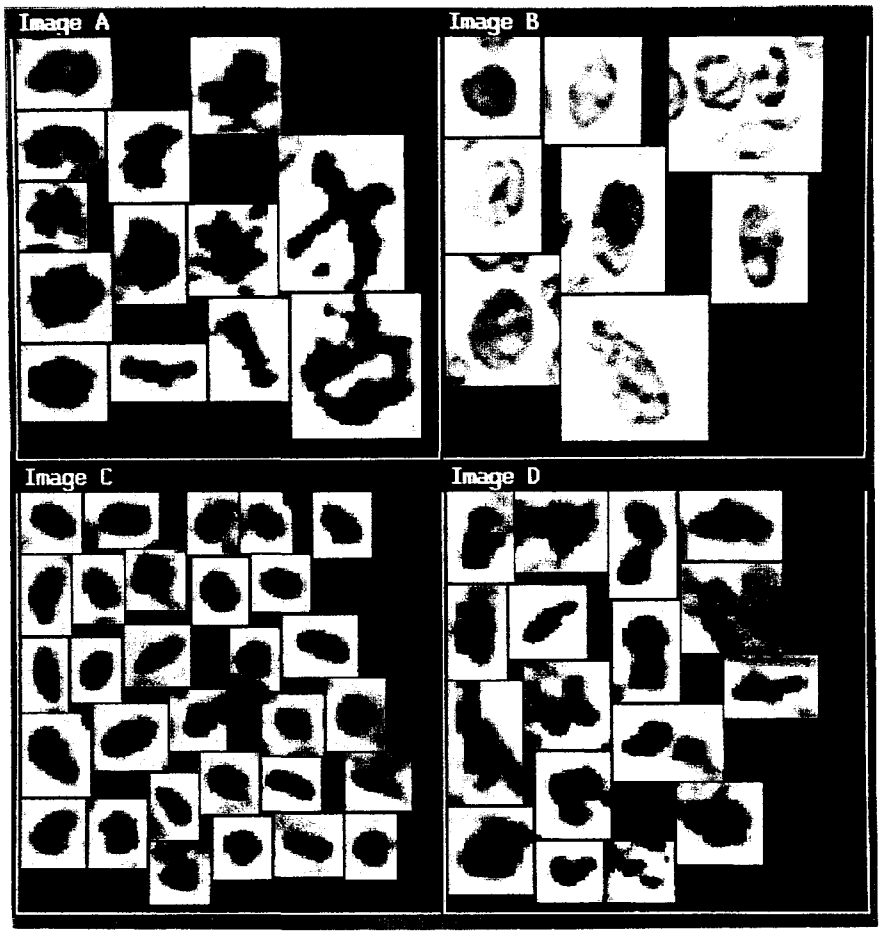

FIG. 3. Image databases containing the four classes of objects: **A.** mitoses, **B.** nuclei, **C.** nuclei of inflammatory cells, **D.** artefacts.

points are included according to the described region grow procedure.

3. Reduction of objects. Objects were excluded from further analysis if they were too small (AREA < 8.1 μm^2) or too large (AREA > 96.1 μm^2), under the reasonable assumption that objects of these dimensions are not mitotic nuclei.

4. Object features. Of the remaining objects, the following grey value features were measured: the optical mass (ODMASS), the average optical density (ODMEAN), the standard deviation of optical density (ODSTDEV). In addition the minimum grey value of the object (MINGREY) was determined as well as a measure for the homogeneity (HOMOG) (32). Beside the area (AREA) and the perimeter (PERI), the bending energy along the contour (BEND) (33) was determined. The bending energy is especially effective in the detection of irregularities in the contour, anticipating the presence of the hairy extensions of the mitotic figures. Along with these features, the contour ratio (CRAT) was computed, which is a measure of the deviation from a perfect circular object. The nine specimens of the learning set were scanned to construct four classes of image databases containing: (1) mitoses, (2) nuclei, (3) artefacts, and (4) nuclei of inflammatory and necrotic cells (hereafter denoted as deviates). The numerical features were stored in a separate database, including the position of the object on the slide to allow for relocation and visual verification through the microscope.

5. Object classification. Classification was done using a Fisher linear discriminant (FLD) rule. The rule found in the learning phase favouring the class of mitosis was implemented in the specimen screening system to test the overall performance at the specimen level.

It is important to avoid counting in inflammatory fields and necrotic areas. The detection of such areas is implemented in the method as follows. A field is suspected and excluded from further analysis when more objects than a fixed threshold are present and the criteria of size, roundness, and homogeneity are fulfilled.

The entire training set was manually screened to gather evenly and randomly objects in all four classes and store them in separate image databases (see Fig. 3)

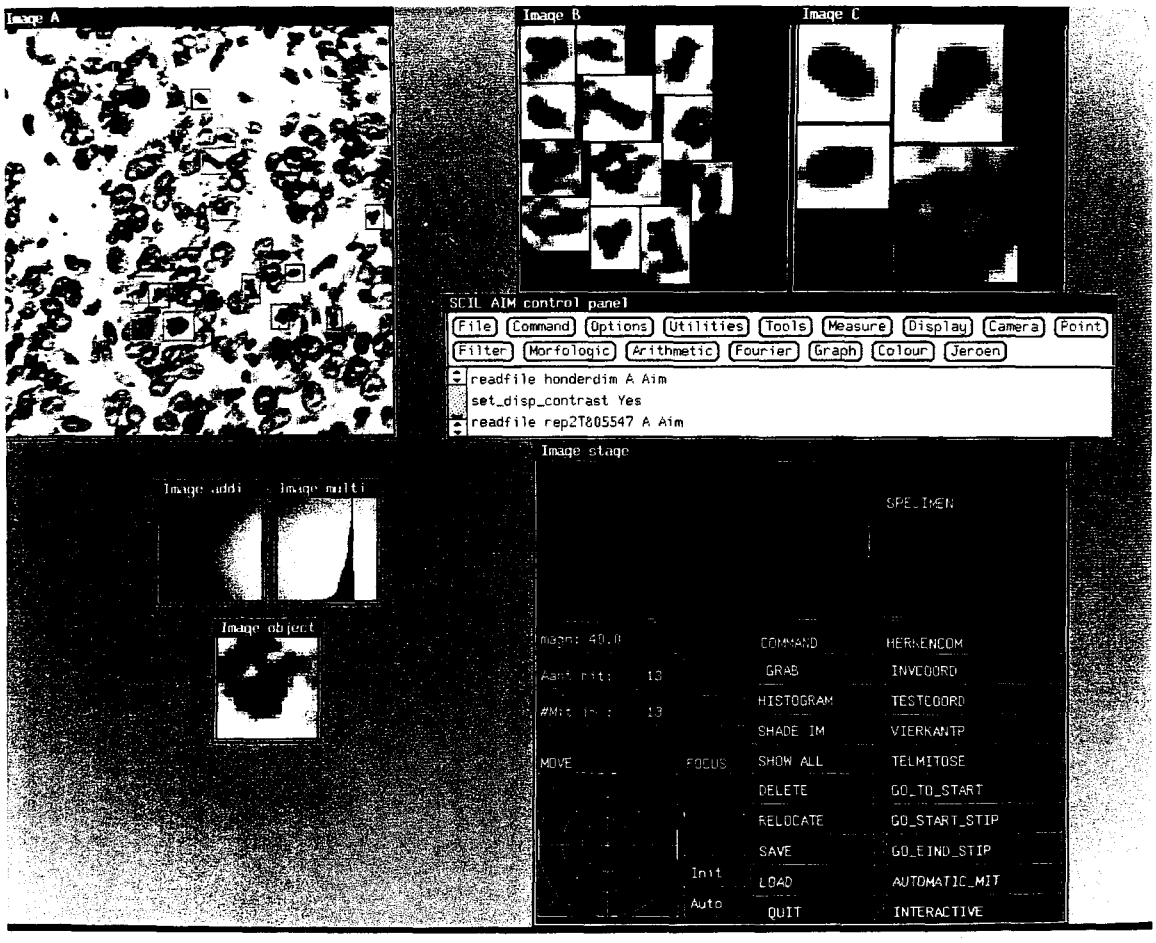

FIG. 4. End-user application for the (semi-)automated detection of mitoses.

to obtain a representative population of all four different objects. Classification was performed at the object level with this training set resulting in the first FLD rule. This FLD rule was then implemented in the program to screen the nine specimens once again, now on an area preselected by a trained technician and by an exhausting search on all objects that fulfil the criteria for either class.

The objects found were first put in two image databases, one for mitoses and one for nonmitoses. A separate program read and displayed the two saved image databases and gave the user the opportunity to select an object of the original database and put it into one of the four new databases (mitoses, cells, artefacts, and deviates). Thereafter, classifications were subsequently checked by an experienced histopathologist on erroneously placed objects. Using this new classification at the object level, a new FLD rule was developed to separate these four groups favouring the class of mitoses by keeping as many mitotic figures in the mitotic class as possible.

This second (final) FLD rule (see Appendix) was used to update the decision rule. Next, the program was exercised over the selected areas of the entire training set at the specimen level. The test set, consisting of the three slides put aside, was scanned as a practical experiment. The mitoses and nonmitoses automatically found by the system were presented to the user in composite images to allow for interactive evaluation. Simultaneously the slides were relocated to the precise object positions to permit visual verification through the microscope; the application is shown in Figure 4. A similar visual interaction has been successfully applied in other studies as well (6). Two observers independently screened the image databases for mitoses. When in doubt, the object was not regarded as a mitosis.

RESULTS

The results of the analysis of the objects gathered manually by selecting the object on the computer screen and storing the selected image part in an image database are given in Table 1. To avoid bias, objects were assembled as evenly and randomly as possible over the slides, not maximizing per slide. The confusion matrix in Table 1 gives an estimate of the correct recognition rate achievable in practice. After step 2a,

Table 1
Confusion Matrix for the Interactively Obtained Objects[a]

	Pre-processing	Nuclei	Artifacts	Deviates	Mitoses	Total
Nuclei	250	25	0	0	0	275
Artefacts	30	0	9	0	10	49
Deviates	6	0	5	33	37	81
Mitoses	0	0	12	6	167	185

[a]After processing and classification, where preprocessing shows the number of objects that are eliminated setting a rigorous low threshold to be used for region growing.

~90% of the nuclei, 60% of the artefacts, and 7% of deviates were excluded, whereas none of the mitoses was eliminated. In the classification analysis that followed, nearly 10% of the mitoses were lost, whereas none of the nuclei, 20% of the artefacts, and 46% of the deviates were incorrectly classified as mitosis.

The classification results of the second, more realistic experiment, where the objects have been automatically selected from slides using the FLD rule obtained from the first training experiment, are given in Table 2. The classification of the mitoses degraded from a net loss of 10–21%, whereas the mitosis class contained 27% of all the nonmitoses. The number of mitoses in Tables 1 and 2 are almost the same, but this is pure coincidence. The mitoses found in the first training experiment were randomly and evenly selected from the entire tissue area to obtain representative images, but in the second test experiment, all the mitoses in the predefined areas were examined. This also holds for the artefacts and deviates. In the first training experiment, only representative objects were gathered, but in the second test, all the objects in the predefined area matching the features were gathered, resulting in larger groups. This explains the difference in false negative rates of Tables 1 and 2. At the specimen level, using the second FLD rule, the results were consistent with the previous values; see Table 3a. In total, 19% (37 of 199) of the detected mitoses were erroneously classified in the first training experiment, whereas overall 30% (24 of 80) of the nonmitoses remaining after the segmentation process were incorrectly classified in the second test experiment (Table 3b). Table 3a also indicates that 11% (25 out of 224) of the mitoses were missed when compared with the interactive counting procedure. The error rates on the test slides, Table 3b, were compatible with those of the training set.

To evaluate the outcome of the image processing, the fully automatic mitoses counting (AMIT) and the automatic mitoses counting followed by an interactive step (AIMIT) were compared with interactively counting of mitoses (1,2), see Figure 5. The figure demonstrates an excellent correlation for both procedures. However, the fully automatic procedure (R = 0.980) would lead to a shift in classification for two specimens.

Table 2
Confusion Matrix for the Automatically Selected Objects[a]

	Nuclei	Artefacts	Deviates	Mitoses	Total
Nuclei	28	12	5	4	49
Artefacts	17	219	71	212	519
Deviates	41	227	608	257	1133
Mitoses	0	17	23	148	188

[a]After image processing and classification, using the FLD found in experiment 1.

The automatic analysis combined with an interactive step is nearly perfect, with a correlation coefficient of 0.998. Finally, the image processing was related to the interactive MAI assessments performed on the HE sections as displayed in Figure 6. To this end, the values of the automatic assessments (AIMAI) were normalized to 10 high power fields to be comparable with the interactive MAI values. The results of both methods were highly comparable (R = 0.990). The formula for calculation of the AMIT is given in the Appendix.

DISCUSSION

The objective of this study was to investigate the potential of image processing for semiautomated mitoses counting in tissue sections. At present, mitoses counting is done interactively by a human observer. To reach sufficient accuracy, a considerable number of fields has to be analyzed, and ongoing motivation and concentration is required.

Although the mitotic count has been widely accepted as a prognostic indicator for malignancy of tumors, the main criticism on mitosis counting has been focused on the (assumed) lack of reproducibility due to the subjective nature of the procedure (8,9,27,34). Nonetheless, the variance in the level of mitotic activity assessments may be kept within reasonable limits by applying a strict protocol (19,21). Under all circumstances, however, evaluation of the mitotic count remains a subjective, tedious, and time-consuming task. Therefore, we have explored the possibilities of automating this task employing image processing.

To our knowledge, there have been few attempts to assess the mitotic rate automatically. A few studies have been dedicated to the standardization of the mitotic activity index (12,15) or to the issue of how many microscopic fields need to be counted (34). A special silver staining has been described (5), which is claimed to facilitate the recognition of mitoses. However, the stain suffers from the fact that stroma and inflammatory cells are also stained. Since these tissue components are particularly difficult to avoid in the analysis, the automation value of this stain is unclear. In addition, in a bladder tumor study (30), this staining method succeeded in preparing specimens suitable for analysis in only ~70%.

Kaman et al. (16) described an attractive approach for detecting mitoses by image processing. However, practical and methodological difficulties stood in the

Table 3

Analysis with Automatic Classification, Automatic Analysis Followed by Interactive Step, and Absolute Observer Agreement Counted Manually (all in identical microscopical fields)

	Automatic analysis		Automatic analysis with interactive evaluation			
Specimen	Mitoses	Non-mitoses	Mitoses	Mitoses classified as nonmitoses	Interactive counting	# Fields
(a) Training Set						
1	81	133	22	9	31	36
2	33	59	14	2	19	40
3	18	63	1	2	4	36
4	36	70	0	1	2	36
5	52	160	1	0	2	34
6	119	75	64	10	81	16
7	122	73	55	6	70	41
8	39	110	4	1	5	43
9	48	212	1	6	10	40
Total	548	955	162	37	224	
(b) Test Set						
10	86	298	2	2	4	50
11	155	173	44	18	71	63
12	47	99	10	4	18	71
Total	288	570	56	24	93	

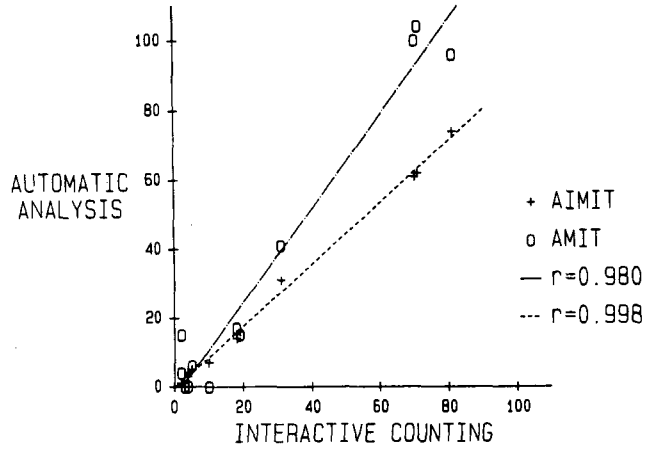

FIG. 5. Results of the image processing related to the manually counting procedure. On the vertical axis the fully automatic image analysis (AMIT) and the image analysis followed by interactive evaluation (AIMIT).

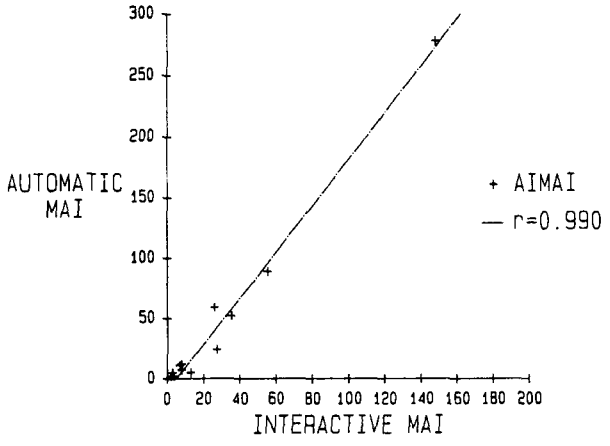

FIG. 6. Results of the automatic analysis related to the interactive morphometric method. The measurements are expressed in the mitotic activity index (MAI).

way of useful implementation. Their result of 37% loss of mitoses may best be compared with the 10% misclassification in Table 1, where it is important to note that our Table 1 was arrived at with low resolution.

In breast cancer sections, the prognostically relevant area of the tumor for mitoses counting comprises $\sim 10^7$ pixels, containing ~5,000–10,000 nuclei. In our method, the detection of mitoses is facilitated by eliminating 95–98% of the nonmitoses. In this process, 10% of the mitoses also were lost. The main reason for loosing a mitosis is low optical density (thereby not surviving the initial threshold), or small size because of sectioning and lying on the edge of the scan field. In the automatic classification procedure, 80% of the mitoses were retained. Probably, operating at relatively low resolution, the discrimination between mitoses and nonmitoses is weakened as contour features are less pronounced compared to high resolution.

For the breast specimens used in this study, the image processing method mainly gives satisfactory results. When related to the interactive counting procedure, the correlation was strong (R = 0.98). However, for specimens with a low number of mitoses, the fully automatic procedure led to a significant discrepancy in

two out of the 12 cases. Therefore, at present, interactive evaluation of the results of automatic procedure is required and gives an almost perfect correlation (R = 0.998) with the mitotic activity index determined through interactive morphometry.

It may be concluded that the fully automated method gives satisfactory results but is not yet suited for clinical practice, whereas the semiautomated method gives reliable results and may be used as a prescreening device. It offers advantages over the interactive assessment of the mitotic count in that it can further improve reproducibility due to the fact that the program records coordinates of the scanned area. So the program can be run during the night to reduce the workload. Whenever necessary, the automatically detected objects classified as mitoses can be displayed on the screen on the monitor and automatically relocated for direct inspection in the microscope. An improvement in the detection of mitoses may be expected using higher resolution, as the shape of the mitoses are better resolved, at the expense, however, of a slower performance. Further improvement may be obtained by using an epithelium specific stain such as CAM 5.2, an anticytokeratin 8 and 18 marker (Becton & Dickinson). Such a stain provides more effective discrimination between epithelium and stroma. Finally, a proper mitosis-enhancing staining procedure might facilitate the recognition of mitotic figures.

ACKNOWLEDGMENTS

The authors thank Conny van Galen for her skilled assistance in the interactive counting of mitosis, and Dr. Paul J. van Diest for critically reading the manuscript.

APPENDIX

Fisher Linear Discriminant rule

The final discrimination rule used in the application is:

Object detected is classified as a cell when:
−.001*ODMASS + .412*ODMEAN +
.618*ODSTDEV + .003*MINGREY + .001*AREA
+ −.001*PERI + .059*CRAT + −.00002*BEND +
−.667*HOMOG > CELTRESH

as an artefact when: −.003*ODMASS +
−.069*ODMEAN + 0.0*ODSTDEV +
−.002*MINGREY + −.001*AREA + .012*PERI +
−.593*CRAT + 0.0*BEND + −.802*HOMOG >
ARTTRESH

and as a deviate when: −.003*ODMASS +
.68*ODMEAN + −.464*ODSTDEV +
.003*MINGREY + .001*AREA + .003*PERI +
−.130*CRAT + −.00005*BEND + .552*HOMOG >
DEVTRESH

where ODMASS, ODMEAN, and ODSTDEV stand for sum, mean, and standard deviation of the integrated optical density, MINGREY for minimum grey value, PERI for perimeter, CRAT for contour ratio, BEND for bending energy, and HOMOG for homogeneity. CELTRESH = 0.073674; ARTTRESH = −1.2028; DEVTRESH = 0.61822. If an object does not fulfill one of these three rules, the object is classified as a mitosis.

AMIT

The AMIT can be found by using the following linear equation:

$$\text{AMIT} = \frac{(1 - \beta) * \text{MIT} - \beta * \text{NON}}{(\alpha - \beta)}$$

were alpha = 1, beta = 0.23, MIT is the number of Mitoses and NON the number of Nonmitoses found with the Automatic analysis (as shown in Table 3a). This linear equation corrects the number of Mitoses found automatically by a percentage of the number of Nonmitoses found automatically. The total number of Nonmitoses found is an indication of the number of false positives.

LITERATURE CITED

1. Baak JPA, Dop H van, Kurver HJ, Hermans J: The value of morphometry to classic prognosticators in breast cancer. Cancer 56:374–382, 1985.
2. Baak JPA, Oort J: Obtaining quantitative data. In: A Manual of Morphometry in Diagnostic Pathology. Baak JPA, Oort J (eds). Springer-Verlag, Berlin, 1983.
3. Baak JPA: Mitosis counting in tumors (editorial). Hum Pathol 21:683–685, 1990.
4. Berryman I, Sterret GF, Papadimitriou JM: Feulgen DNA cytophotometry in histologic sections of mammary neoplasms. Anal Quant Cytol 6:19–23, 1984.
5. Busch C, Vasko J: Differential staining of mitoses in tissue sections and cultured cells by a modified methenamine-silver method. Lab Invest 59:876–878, 1988.
6. Cornelisse CJ, Driel-Kulker AM van: DNA image cytometry on machine-selected breast cancer cells and a comparison between flow cytometry and scanning cytophotometry. Cytometry 6:471–477, 1985.
7. Chaudhuri BB, Rodenacker K, Burger G: Characterization and featuring of histological section images. Pattern Recogn Letters 7:245–252, 1988.
8. Diest PJ van, Baak JPA, Matze-Cok P, Wisse-Brekelmans ECM, Galen CM van, Kurver PHJ, Bellot SM, Fijnheer J, Gorp LHM, Kwee WS, Los J, Peterse JL, Ruitenberg HM, Schapers RFM, Schipper MEI, Somsen JG, Willig AWPM, Ariens ATh: Reproducibility of mitosis counting in 2,469 breast cancer specimens: Results from the Multicenter Morphometric Mammary Carcinoma Project. Hum Pathol 23:603–607, 1992.
9. Donhuijsen K: Mitosis counts: Reproducibility and significance in grading of malignancy. Hum Pathol 17:1122–1125, 1986.
10. Donhuijsen K, Schmidt U, Hirche H, Beuningen D van, Budach V: Changes in mitotic rate and cell cycle fractions caused by delayed fixation. Hum Pathol 21:709–714, 1990.
11. Duijndam WAL, Duijn P van: The interaction of apurinic acid aldehyde groups with pararosaniline in the Feulgen-Schiff and related staining procedures. Histochemistry 44:67–85, 1975.
12. Ellis PSJ, Whitehead R: Mitosis counting-a need for reappraisal. Hum Pathol 12:3–4, 1981.
13. Fu YS, Hall TL: DNA ploidy measurements in tissue sections. Anal Quant Cytol Histol 7:90–95, 1985.
14. Gelsema ES: ISPAHAN: An interactive system for pattern analysis; structure and capabilities. In: Pattern Recognition in Practice. Gelsema ES, Kanal LN (eds). North-Holland, Amsterdam, 1980, pp 481–491.

15. Haapasalo H, Pesonen E, Collan Y: Volume corrected mitotic index (m/v-index). The standard of mitotic activity in neoplasms. Path Res Pract 185:551–554, 1989.
16. Kaman EJ, Smeulders AWM, Verbeek PW, Young IT, Baak JPA: Image processing for mitoses in sections of breast cancer: A feasibility study. Cytometry 5:244–249, 1984.
17. Kate TK ten, Balen R van, Smeulders AWM, Groen FCA, Boer GA den: SCILAIM: A multi-level interactive image processing environment. Pattern Recogn Letters 11:429–441, 1990.
18. Kate TK ten, Smeulders AWM: Accuracy of optical density measurements of cells II. High resolution (submitted).
19. Kempson RL: Mitosis counting-II (editorial). Hum Pathol 7:482–483, 1976.
20. Lee T-K, Myers RT, Marshall RB, Bond MG, Kardon B: The significance of mitotic rate: A retrospective study of 127 Thyroid carcinomas. Hum Pathol 16:1042–1046, 1985.
21. Norris HJ: Mitosis counting-III (editorial). Hum Pathol 7:483–484, 1976.
22. Pesce CM: Biology of disease. Defining and interpreting diseases through morphometry. Lab Invest 56:568–575, 1987.
23. Ridler TW, Calvard S: Picture thresholding using an iterative selection method. IEEE Trans Sys Man Cyber SMC-8:630–632, 1978.
24. Schipper NW, Smeulders AWM, Baak JPA: Evaluation of automated estimation of epithelial volume and its prognostic value in ovarian tumors. Lab Invest 61:228–234, 1989.
25. Schipper NW, Smeulders AWM, Baak JPA: Quantification of epithelial volume by image processing applied to ovarian tumors. Cytometry 8:345–352, 1987.
26. Schipper NW, Smeulders AWM, Lange JHM de, Baak JPA: Quantification of epithelial area by image processing applied to endometrial carcinomas: A comparison with ovarian tumors. Hum Pathol 20:1125–1132, 1989.
27. Silverberg SG: Reproducibility of the mitosis count in the histologic diagnosis of smooth muscle tumors of the uterus. Hum Pathol 7:451, 1976.
28. Sowter C, Slavin G, Rosen D: Morphometry of bladder carcinoma: I. The automatic delineation of urothelial nuclei in tissue sections using an IBAS II image array processor. J Pathol 153:289–297, 1987.
29. Stenkvist B, Bengtsson E, Eriksson O, Jarkrans T, Nordin B, Westman-Naeser S: Correlation between cytometric features and mitotic frequency in human breast carcinoma. Cytometry 1:287–291, 1981.
30. Vasko J, Malmstrom P-E, Wester K, Busch C: Prognostic value of standardized determination of mitotic frequency in bladder cancer using image analysis (submitted).
31. Wied GL, Bartels PH, Bibbo M, Dytch HE: Image analysis in quantitative cytopathology and histopathology. Hum Pathol 20: 549–571, 1989.
32. Young IT, Verbeek PW, Mayall BH: Characterization of Chromatin Distribution in Cell Nuclei. Cytometry 7:467–474, 1986.
33. Young IT, Walker JE, Bowie JE: An analysis technique for biological shape. I Inf Control 25:357–370, 1974.
34. Zuckman MH, Williams G, Levin HS: Mitosis counting in seminoma: An exercise of questionable significance. Hum Pathol 19: 329–335, 1988.